Probing Moiré Bloch Bands of Photoexcited Electrons on Graphene/Ir(111)

Ryuichi Arafune [1], Hiroshi Ishida [2], Chun-Liang Lin [3] and Noriaki Takagi [4]

[1] *Research center for materials nanoarchitectonics (MANA), National Institute for Materials Science (NIMS), Tsukuba, Japan**

[2] *College of Humanities and Sciences, Nihon University, Tokyo, Japan*

[3] *Dept. of Electrophysics, National Yang Ming Chiao Tung University (NYCU), Hsinchu City, Taiwan*

[4] *Graduate School of Human and Environmental Studies, Kyoto University, Kyoto, Japan*

(Dated: October 3, 2025)

Abstract

We have investigated the moiré Bloch bands of photoexcited electrons in image potential states (IPS) on graphene covered Ir(111) surfaces using high-energy-resolution angle-resolved two-photon photoemission spectroscopy. An energy gap of approximately 20 meV at the $\bar{\mathrm{K}}$ point of the moiré Brillouin zone is resolved. The band structure is well reproduced by density functional theory (DFT) combined with the embedded Green's function technique. A simplified periodic potential model, whose spatial distribution shows close agreement with the DFT results, also describes the system well. These findings demonstrate that the electronic band structure of photoexcited states can be engineered solely via moiré potential modulation. This opens a new avenue for excited-state band engineering and the design of ultrafast optoelectronic functionalities in moiré-engineered materials.

When a two-dimensional (2D) material is grown on a crystalline surface, or when multiple 2D materials are stacked with a mismatch in their lattice periodicities or orientations, spatial interference patterns known as moiré structures emerge[1]. Although moiré structures were once appreciated mainly for their geometric aesthetics and usefulness in structural analysis[2], their functional significance has come into focus more recently. In particular, novel electronic transport phenomena arising from the moiré superlattice, such as the emergence of superconductivity and Mott insulating states in twisted bilayer graphene at so-called "magic angles" [3, 4] and fractal electronic spectra known as Hofstadter's butterfly [5], are regarded as one of the most impactful advances in condensed matter physics in the past decades.

The relevance of moiré superlattice have been recognized also in optical processes. For example, spatially localized excitons in moiré superlattices formed by stacked transition metal dichalcogenides[6] has opened new possibilities for controlling photoexcitation and light–matter interactions. However, in contrast to electronic transport, the implications of moiré effects in optical phenomena remain poorly understood. To gain a deeper understanding of such optical properties, it is important to focus on moiré Bloch bands[7], which played a crucial role in explaining exotic electronic behavior. These miniband structures, formed via hybridization of electronic states under the long-range periodic potential of the moiré pattern, may also be key to understanding moiré-modified light–matter interactions.

* ARAFUNE.Ryuichi@nims.go.jp

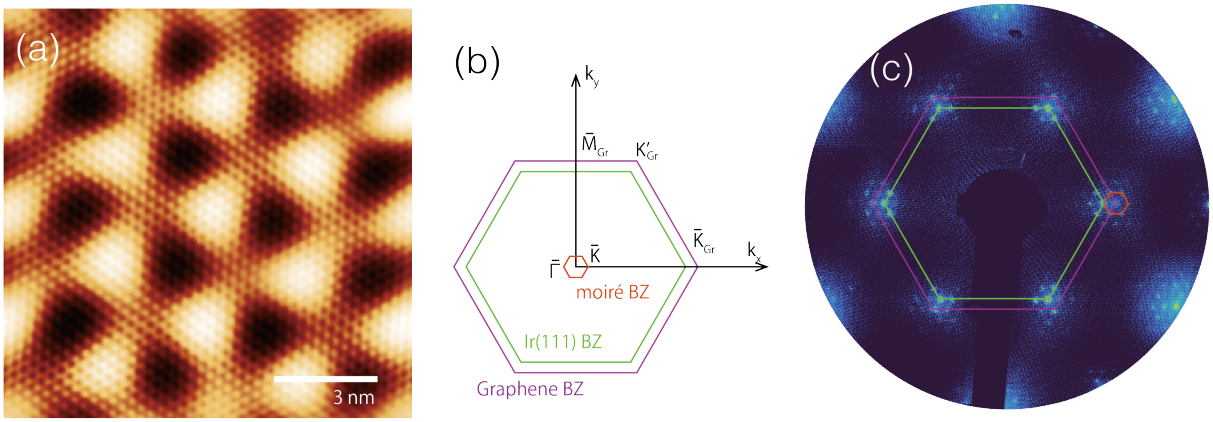

FIG. 1. (a) Scanning tunneling microscope (STM) image of graphene covered Ir(111) (Gr/Ir(111)) surface, showing the formation of long-period moiré superlattice due to the lattice mismatch between graphene and Ir(111) surface. The bias voltage and the tunneling current were set to -80 mV and 1.2 nA, respectively. (b) Brillouin Zones (BZs) of the Ir(111) surface and graphene lattices, drawn to scale. The moiré BZ, indicated by the red hexagon, shows a significantly reduced size, enabling the emergence of miniband. (c) LEED picture of Gr/Ir(111), showing sharp diffraction spots from Ir, carbon and the surrounding moiré satellites, indicating high structural quality and uniformity of the sample surface.

In this Letter[8], we report the experimental observation of moiré Bloch bands of photoexcited electrons in image potential states (IPS) on the graphene-covered Ir(111) (Gr/Ir(111)) surfaces (Fig. 1), by using high-resolution angle-resolved two-photon photoemission (HR-AR2PPE) spectroscopy [9, 10]. As shown in Fig. 1(a), Gr/Ir(111) provides a well-defined moiré superlattices with a periodicity of approximately 25 Å, which is much larger than the lattice constant of graphene (2.46 Å) and Ir(111) (2.72 Å) [11, 12]. It is widely accepted that the (10×10) supercell of graphene on the (9×9) cell of Ir(111) well describes the Gr/Ir(111) superlattices, with the lattice vectors of graphene and Ir(111) being aligned in orientation [11, 12]. Thus, the Brillouin zones (BZ) of these two surfaces and resulting moiré BZ are drawn as shown in Fig. 1(b). IPS are quantized electronic states formed by the Coulomb attraction between an electron and its induced image charge at a metallic surface. Owing to their well-defined nature and surface sensitivity, IPS serve as an ideal platform for investigating photoexcited carrier dynamics, including energy relaxation and quantum

interference phenomena on solid surfaces[13, 14]. We expected that their surface sensitivity makes IPS particularly suitable for probing moiré potential effects, such as the formation of moiré bands in photoexcited states. Previous works investigated IPS on graphene-covered metal surfaces[15–20], revealing the energy positions, lifetimes, and the effective masses. On certain metal surfaces such as the Ru(0001), graphene forms a relatively large rippled structure, which leads to a band splitting of the IPS state[15]. However, the effect of the moiré superlattice on the electronic structure of IPS has not been fully explored, and, to our knowledge, the opening of a gap in the moiré Bloch bands of the unoccupied states has not been reported. This motivates our present study on Gr/Ir(111) IPS, where we directly probe the moiré-induced electronic reconstruction in the unoccupied states

The experimental setup consisted of a laser system and an ultra-high vacuum (UHV) electron spectroscopy system. A Ti:sapphire laser oscillator generated infrared (IR) pulses with 2.0 ps duration at 80 MHz. Part of the IR output was converted to ultraviolet (UV) light using nonlinear crystals. P-polarized IR and UV pulses were aligned collinearly and focused onto the sample. Two-photon photoemission (2PPE) measurements were conducted in an ultra-high vacuum system with a base pressure below 7×10^{-11} mbar. The sample temperature was held at 11 K during the measurements. Energy and momentum resolutions were 9.5 meV and better than 0.01 Å^{-1}, respectively. Graphene was grown by a two-step thermal decomposition of ethene [11, 21] on the clean Ir(111), confirmed by a sharp moiré induced spots in low energy electron diffraction (LEED) as shown in Fig. 1(c). First-principles calculations were performed using density functional theory (DFT) combined with the embedded Green's function and full-potential linearized augmented plane-wave methods[22–25] for modeling graphene on the semi-infinite Ir(111) substrate. The DFT potential $\bar{V}_{\text{eff}}(z)$ was smoothly matched to a classical image potential[26] to describe IPS. Experimental and computational details are provided in the Supplemental Material[8], which includes the following literatures [10, 11, 21–37].

Figure 2 shows the HR-AR2PPE spectra for the first IPS of Gr/Ir(111). The pump and probe photon were 4.401 and 1.467 eV, respectively. At normal emission, the peak was located at 5.308 eV with a width of 56 meV, indicating the binding energy of IPS with respect to the vacuum level is -0.849 eV (The workfunction determined from the vacuum level cutoff was 4.69 eV.). Unlike the 2PPE data of IPS on noble metal such as Cu(001) and Ag(001), the maximum intensity does not occur at the bottom of the band. This strong

intensity originates from the surface resonances of the Ir(111) in the occupied region [37]. This surface resonance is known as a Rashba-type spin-split hole-like band. Although the intensity is weak, photoelectrons coherently excited from the surface resonance state are indeed observed[8]. These values and features are consistent with the previous report [17].

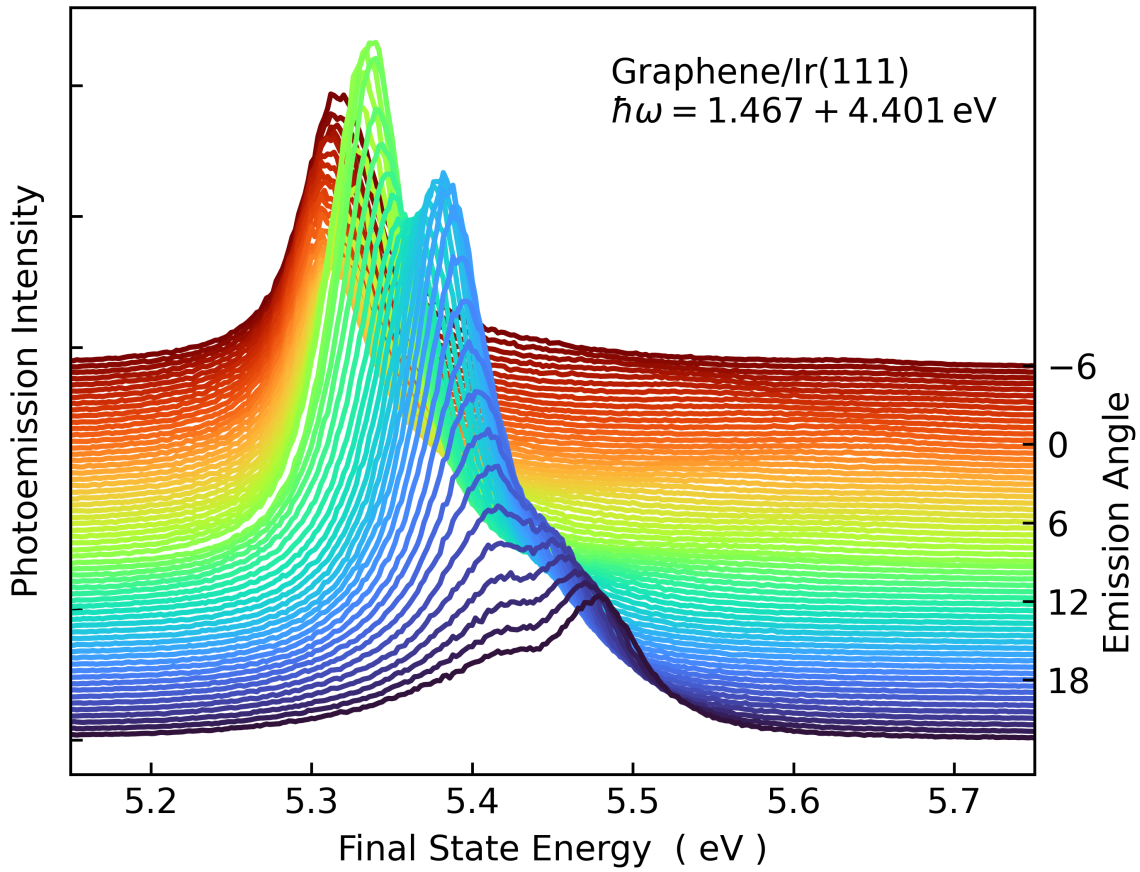

FIG. 2. Angle resolved two-photon photoemission spectra of graphene covered Ir(111). At low angles, a single peak appears at around 5.3 eV final-state energy. The final state energy refers to the excited state energy measured from the Fermi level. As the emission angle increases, a shoulder emerges and evolves into a pronounced double-peak structure, clearly visible at 23°, indicating an energy gap of ∼20 meV at the $\bar{\mathrm{K}}$ point of the moiré BZ. This angular-dependent splitting provides direct experimental evidence of the formation of moiré Bloch bands in the unoccupied electronic structure.

Importantly, while a single peak is observed at low emission angles, the spectra exhibit a

pronounced double-peak structure at higher emission angles. As the emission angle increases, a shoulder starts to develop around 17°. At 23°, the spectrum clearly exhibits a double-peak structure, with an energy separation of 62 meV between the peaks. This splitting clearly demonstrates the presence of an energy gap in the unoccupied electronic states, providing direct experimental evidence of the moiré-induced band modification. By spectral fitting using two Lorentzian curves, we have evaluated the energy gap at the $\bar{\mathrm{K}}$ point of the moiré BZ to be 20 meV[8].

Figure 3 shows the log-intensity map of the electronic structure of moiré Bloch band arising from IPS of Gr/Ir(111). This data is obtained form the HR-AR2PPE spectra taken by using another photon energy pair: 1.600 + 4.800 eV. The measured IPS spectra along the k_x direction (along $\bar{\Gamma}$-$\bar{\mathrm{K}}$, see Fig. 1(b)) show the energy splitting induced by the moiré potential. We confirmed that the location of the energy gap in the momentum axis and its magnitude are essentially independent of the excitation photon energy. Furthermore, one can see the folded band appears well. These features also clearly imply a robust feature of the moiré superlattice.

The emergence of the moiré band with an energy gap is supported by DFT calculations. In supplemental materials[8], the calculated band dispersion was imposed on the experimental results (see. Fig. S3). Since the band splitting due to spin-orbit coupling was less than a few meV, we plotted the energy dispersion averaged over two spin components. The calculated energy levels have been shifted upward by 80 meV to align the experimental results. Note that the actual binding energy discrepancy between the experimental and theoretical energy values is larger when considered relative to the vacuum level. The calculated work function was 4.847 eV, resulting in a binding energy discrepancy of -89 meV. The calculated energy gap at the $\bar{\mathrm{K}}$ point of the moiré BZ was 22 meV. Although the energy values does not precisely reproduce the experimental results, the overall band structure shows good agreement with the measurements.

Since the electron in IPS essentially behaves as the free electron, the moiré Bloch band arising from IPS is expected to be well described by a simplified nearly free-electron (NFE) model under a periodic moiré potential. By fitting the DFT-calculated dispersion, we obtain an effective mass equal to the free-electron mass, along with a complex Fourier coefficient of the moiré potential V: $V = \alpha + i\beta$, where $\alpha = 7.5$ meV and $\beta = 1.1$ meV. This confirms that the essential features of the moiré band, including the energy gap at the $\bar{\mathrm{K}}$ point, can

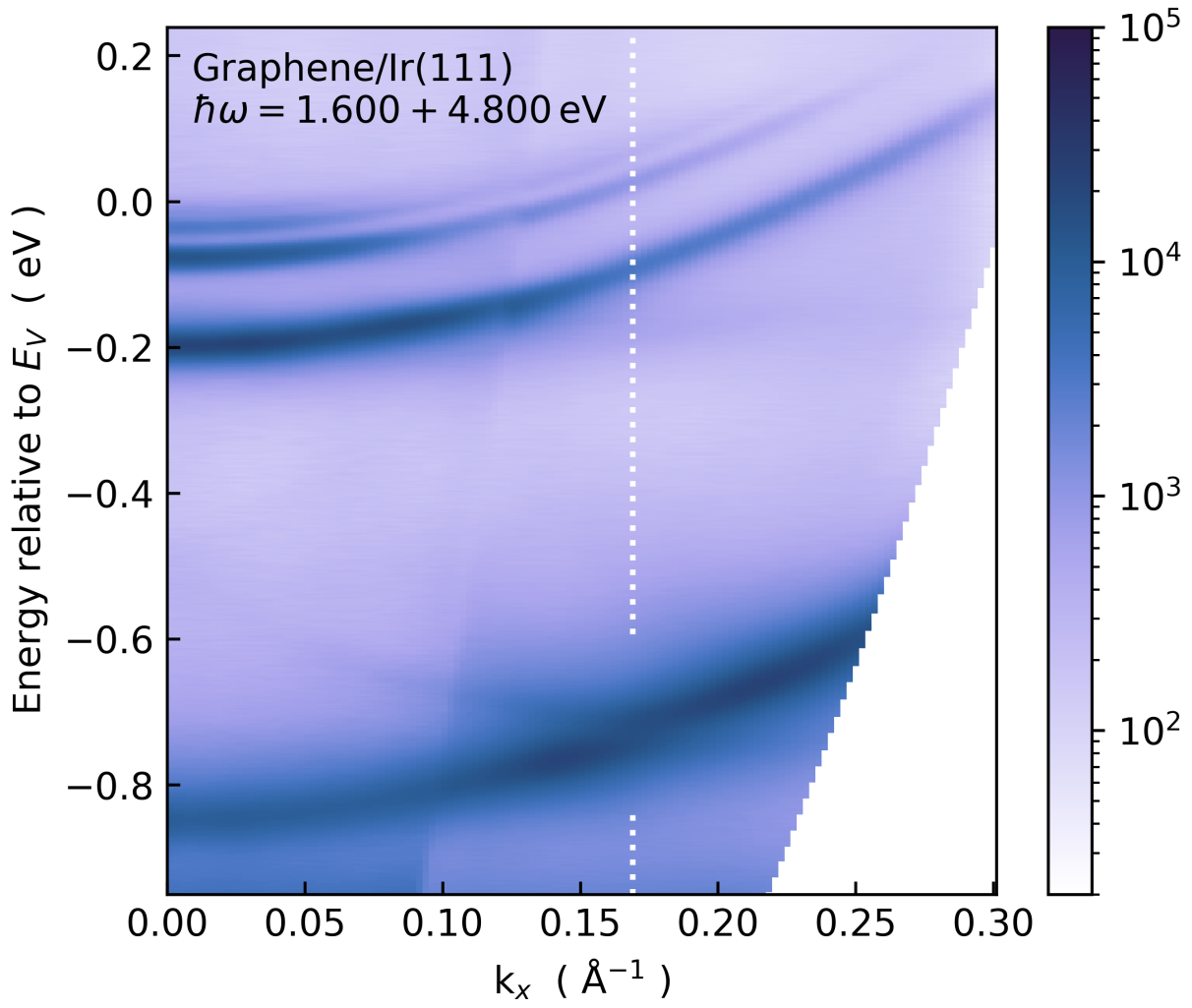

FIG. 3. A log-intensity map of electronic structure of moiré Bloch band arising from IPS of Gr/Ir(111). The k_x direction is along the $\bar{\Gamma}$-$\bar{\mathrm{K}}$ direction in BZ, as shown in Fig. 1(b). The pump and probe photon energies were 4.800 eV and 1.600 eV, respectively. The vertical dotted line denotes the BZ boundary in the $\bar{\Gamma}$-$\bar{\mathrm{K}}$ direction for the moiré BZ. The folded features match well with the theoretical prediction, despite weak intensity. The clear splitting observed near the $\bar{\mathrm{K}}$ point evidences the opening of a moiré-induced energy gap.

be quantitatively described by NFE model. Details of the model and the resultant fitting curves are provided in the Supplemental Material[8], which shows that the NFE model nearly perfectly reproduces both the experimental and DFT results.

Now let us examine the effective potential landscape induced by the moiré superlattice in the electronic system. Figure 4(a) presents a contour map of the potential distribution

obtained from the NFE model, while Fig. 4(b) shows that derived from DFT calculations. The height of the potential distribution in the plot (b) was determined by referencing the charge density distribution along the surface normal. The first moment of the charge density distribution was found to be 6 Å (Fig. 4(c)), and this value was used as the reference height. While the potential distribution derived from the DFT calculations includes contributions from atomic cores, the overall landscape of the potential is well reproduced by NFE model. The situation $\alpha \gg \beta$ implies that the system is essentially characterized by the sixfold rotational symmetry, and the difference between the hcp and fcc sites in Gr/Ir(111) can be neglected as shown in Fig. 4. This comparison further reinforces the interpretation that the observed energy gap originates from the moiré potential.

As shown in Fig. 3, the energy gap opens in the energy dispersion relation of the first IPS alone, while no gap is observed in the higher order ($n \geq 2$) IPS. This is consistent with the theoretical prediction that the spatial variation of the moiré potential for the higher order IPS is too weak to open the gap. It is well known that the first moment of the wave function, and thus that of the charge distribution, moves farther from the surface as n increases [13, 31]. This means that the electron in the higher order IPS feels a weaker moiré potential, resulting in no gap opening. Indeed, the first moment of the charge distribution for the second IPS is located at around $z \sim 14$ Å in our DFT calculations as shown in Fig. 4(c). Note that in Fig. 4(c), z_b[8] denotes the position above the plane of the embedding surface on the vacuum side. In our calculation, we assume that at this position the potential curve is given by the classical image potential and is independent of x and y. This corresponds to $\alpha = \beta = 0$ in the NFE model, resulting in no energy gap. This result suggests that energy gap can be controlled by tuning the modulation of the moiré potential.

We note that the IPS are free-electron-like states and therefore isotropic in k (i.e., the constant energy surface should be circular). However, the moiré potential is not isotropic and has a specific symmetry (see, e.g., the occupied spectrum in ref.[38]). In the present work, we have measured the spectra only along the $\bar{\Gamma}$–$\bar{\mathrm{K}}$ direction, but measurements along other directions are planned for future studies to further explore the effects of the moiré symmetry on the IPS. Our DFT calculations indicate that the band gap at the $\bar{\mathrm{M}}$ point is about 15 meV, slightly smaller than that at the $\bar{\mathrm{K}}$ point. The NFE model also reproduces this band gap at the $\bar{\mathrm{M}}$ point, although experimental confirmation is still required.

Before concluding, we would like to discuss the impact of the graphene structure on

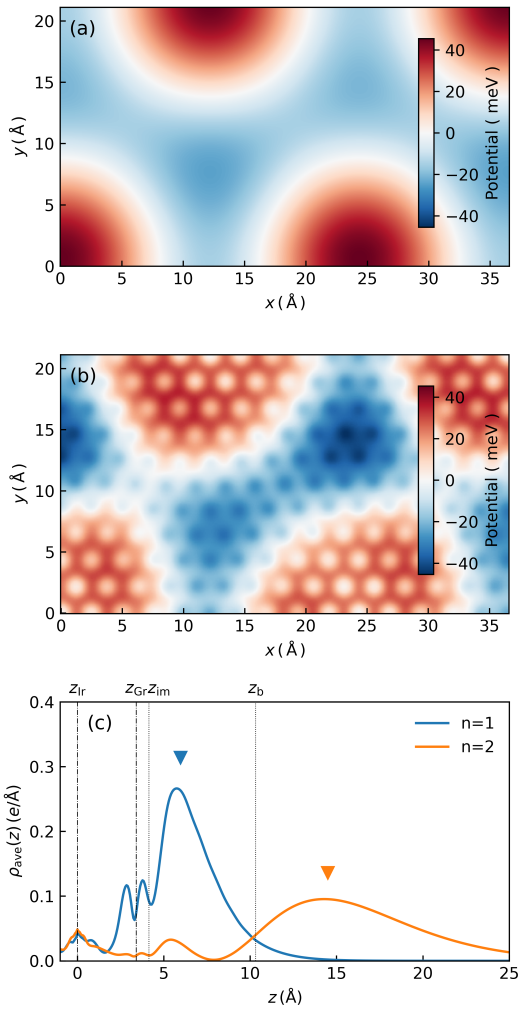

FIG. 4. (a) Contour map of the potential distribution calculated from the nearly free electron model described in the Supplemental Material. (b) Corresponding electrostatic potential distribution at a height of $z = 6$ Å above the Ir substrate, obtained from DFT calculations. The qualitative agreement between (a) and (b) supports the validity of the simplified model. (c) Planar-averaged charge density (ρ) distribution of IPS ($n = 1, 2$) at the $\bar{\text{K}}$ point of the moiré BZ, which is used to determine the effective height for evaluating the lateral potential distribution. The vertical dash dot line at $z = 3.40$ Å indicates the average height of the carbon atoms of graphene. The vertical dot lines at $z = 4.13$ Å and at $z = 10.3$ Å indicate the height of the image plane (z_{im}), and the plane of the embedding surface (z_b), respectively. For $z > z_b$, we model the potential as the classical image potential. The triangles indicate the height corresponding to the first moment of the charge density distribution for IPS (blue: $n = 1$, orange: $n = 2$).

Ir(111) surface. It is well accepted that the graphene forms a rippled structure on the Ir(111) surface [11, 12], and our calculations take this into account. The ripple amplitude is smaller than that of graphene on the Ru(0001)[15]. As a result, we cannot identify the energy splitting, even though the energy resolution of our experimental setup was better than in previous works [16–20]. Nevertheless, the presence of this small ripple structure is still significant. The periodicity of the rippled structure is identical to that of the moiré superlattice. Which of the two, then, is fundamentally responsible for the origin of the gap formation? In this context, we recently have demonstrated that the surface corrugation caused by the surface reconstruction induces the energy gap of IPS[32]. To answer this question, we have performed DFT calculations for flat graphene on the Ir(111) surface. Despite the absence of the rippled structure, an energy gap is still observed in the calculated band dispersion of IPS, and the magnitude of the gap was essentially identical to that of the rippled graphene system. This result indicates that the gap formation originates solely from the geometric moiré structure. Although macroscopic wrinkles may exist due to thermal expansion mismatch between graphene and Ir[39], these features are non-periodic and are unlikely to affect the moiré-induced gap observed in our measurements. This is consistent with the sharp LEED spots across the sample. Beyond confirming the structural origin of the gap, this result implies that moiré potentials can be used to deliberately tailor the unoccupied electronic structure of excited states. This establishes a new conceptual framework for excited-state band engineering using structural moiré design alone, without relying on external fields or chemical modifications.

In conclusion, we have experimentally demonstrated the formation of moiré Bloch bands with an energy gap in the unoccupied image-potential states of Gr/Ir(111), supported by DFT calculations and a simple NFE model. The observed energy gap originates solely from the geometric moiré potential. These findings provide direct evidence that excited-state electronic bands can be modulated by structural moiré design, establishing a new approach to excited-state band engineering. This concept opens a pathway toward ultrafast optoelectronic control in moiré-engineered materials, without requiring chemical doping or external fields.

ACKNOWLEDGMENTS

This work was financially supported by JSPS KAKENHI (Grant Number 22H01960) and the World Premier International Research Center Initiative (WPI) on Materials Nanoarchitectonics, MEXT, Japan. It was also partially supported by the National Science and Technology Council, Taiwan under NSTC 114–2923-M-A49-001-MY2, NSTC 113–2124-M-A49-007, NSTC 113–2628-M-A49-006-MY3, and NSTC T-Star Center Project: Future Semiconductor Technology Research Center under NSTC 114–2634-F-A49-001.

[1] I. Amidror, *The Theory of Moiré Phenomenon*, Computational Imaging and Vision, Vol. 38 (Springer London, 2009).

[2] N. Kawakami, C.-L. Lin, K. Kawahara, M. Kawai, R. Arafune, and N. Takagi, Structural evolution of bi thin films on au(111) revealed by scanning tunneling microscopy, Physical Review B **96**, 205402 (2017).

[3] Y. Cao, V. Fatemi, S. Fang, K. Watanabe, T. Taniguchi, E. Kaxiras, and P. Jarillo-Herrero, Unconventional superconductivity in magic-angle graphene superlattices, Nature **556**, 43 (2018).

[4] Y. Cao, V. Fatemi, A. Demir, S. Fang, S. L. Tomarken, J. Y. Luo, J. D. Sanchez-Yamagishi, K. Watanabe, T. Taniguchi, E. Kaxiras, R. C. Ashoori, and P. Jarillo-Herrero, Correlated insulator behaviour at half-filling in magic-angle graphene superlattices, Nature **556**, 80 (2018).

[5] C. R. Dean, L. Wang, P. Maher, C. Forsythe, F. Ghahari, Y. Gao, J. Katoch, M. Ishigami, P. Moon, M. Koshino, T. Taniguchi, K. Watanabe, K. L. Shepard, J. Hone, and P. Kim, Hofstadter's butterfly and the fractal quantum hall effect in moiré superlattices, Nature **497**, 598 (2013).

[6] K. L. Seyler, P. Rivera, H. Yu, N. P. Wilson, E. L. Ray, D. G. Mandrus, J. Yan, W. Yao, and X. Xu, Signatures of moiré-trapped valley excitons in $MoSe_2/WSe_2$ heterobilayers, Nature **567**, 66 (2019).

[7] R. Bistritzer and A. H. MacDonald, Moiré bands in twisted double-layer graphene, Proceedings of the National Academy of Sciences of the United States of America **108**, 12233 (2011).

[8] See Supplemental Material at `http://xxxx.xxxx.xxx/` for ball-stick-model of graphene cov-

ered Ir(111) surface, details of experimental and computational procedures, $E(k)$ representation of HR-AR2PPE data, and details of the nearly free electron model for the moiré Bloch band.

[9] R. Arafune, N. Takagi, and H. Ishida, Spin-orbit interaction in unoccupied surface states, Progress in Surface Science **93**, 177 (2018).

[10] T. Nakazawa, N. Takagi, M. Kawai, H. Ishida, and R. Arafune, Rashba splitting in an image potential state investigated by circular dichroism two-photon photoemission spectroscopy, Physical Review B **94**, 115412 (2016).

[11] A. T. N'Diaye, J. Coraux, T. N. Plasa, C. Busse, and T. Michely, Structure of epitaxial graphene on Ir(111), New Journal of Physics **10**, 043033 (2008).

[12] S. K. Hämäläinen, M. P. Boneschanscher, P. H. Jacobse, I. Swart, K. Pussi, W. Moritz, J. Lahtinen, P. Liljeroth, and J. Sainio, Structure and local variations of the graphene moiré on Ir(111), Phys. Rev. B **88**, 201406 (2013).

[13] U. Höfer, I. L. Shumay, Ch. Reuß, U. Thomann, W. Wallauer, and Th. Fauster, Time-Resolved Coherent Photoelectron Spectroscopy of Quantized Electronic States on Metal Surfaces, Science **277**, 1480 (1997).

[14] B. Borca and H. J. Zandvliet, Image potential states of 2d materials, Applied Materials Today **39**, 102304 (2024).

[15] N. Armbrust, J. Güdde, P. Jakob, and U. Höfer, Time-Resolved Two-Photon Photoemission of Unoccupied Electronic States of Periodically Rippled Graphene on Ru(0001), Physical Review Letters **108**, 056801 (2012).

[16] D. Nobis, M. Potenz, D. Niesner, and T. Fauster, Image-potential states of graphene on noble-metal surfaces, Physical Review B **88**, 195435 (2013).

[17] D. Niesner, T. Fauster, J. I. Dadap, N. Zaki, K. R. Knox, P. C. Yeh, R. Bhandari, R. Osgood, M. Petrović, and M. Kralj, Trapping surface electrons on graphene layers and islands, Physical Review B **85**, 081402 (2012).

[18] D. Gugel, D. Niesner, C. Eickhoff, S. Wagner, M. Weinelt, and T. Fauster, Two-photon photoemission from image-potential states of epitaxial graphene, 2D Materials **2**, 045001 (2015).

[19] Y. Lin, Y. Li, J. T. Sadowski, W. Jin, J. I. Dadap, M. S. Hybertsen, and R. M. Osgood, Excitation and characterization of image potential state electrons on quasi-free-standing graphene, Phys. Rev. B **97**, 165413 (2018).

[20] Y. Lin, G. Chen, J. T. Sadowski, Y. Li, S. A. Tenney, J. I. Dadap, M. S. Hybertsen, and R. M. Osgood, Observation of intercalation-driven zone folding in quasi-free-standing graphene energy bands, Phys. Rev. B **99**, 035428 (2019).

[21] J. Coraux, A. T. N'Diaye, M. Engler, C. Busse, D. Wall, N. Buckanie, F.-J. M. zu Heringdorf, R. van Gastel, B. Poelsema, and T. Michely, Growth of graphene on Ir(111), New Journal of Physics **11**, 039801 (2009).

[22] H. Ishida, Surface-embedded Green-function method: A formulation using a linearized-augmented-plane-wave basis set, Physical Review B **63**, 165409 (2001).

[23] Inglesfield, John E., A method of embedding, Journal of Physics C: Solid State Physics **14**, 3795 (1981).

[24] D. J. Singh and L. Nordström, *Planewaves, Pseudopotentials, and the LAPW Method*, 2nd ed. (Springer New York, NY, 2006).

[25] H. Ishida, R. Arafune, and N. Takagi, First-principles calculation of the graphene dirac band on semi-infinite Ir(111), Phys. Rev. B **102**, 195425 (2020).

[26] M. Nekovee and J. Inglesfield, Theory of image states at magnetic surfaces, Progress in Surface Science **50**, 149 (1995).

[27] C. Stansbury and A. Lanzara, Pyarpes: An analysis framework for multimodal angle-resolved photoemission spectroscopies, SoftwareX **11**, 100472 (2020), although based on an existing framework, the version of the code used in this study was significantly rewritten by the authors:https://github.com/arafune/arpes.

[28] N. D. Lang and W. Kohn, Theory of Metal Surfaces: Induced Surface Charge and Image Potential, Physical Review B **7**, 3541 (1973).

[29] N. D. Lang, Interaction between Closed-Shell Systems and Metal Surfaces, Physical Review Letters **46**, 842 (1981).

[30] R. O. Jones, P. J. Jennings, and O. Jepsen, Surface barrier in metals: A new model with application to W (001), Physical Review B **29**, 6474 (1984).

[31] Y.-C. Tai, C.-W. Luo, N. Takagi, H. Ishida, C.-L. Lin, and R. Arafune, Coherent multiphoton photoemission spectroscopy of image-potential state on Ir(111) surface, Applied Physics Express **18**, 062001 (2025).

[32] P. Amrit, N. Kawakami, N. Takagi, H. Ishida, C.-L. Lin, and R. Arafune, Gap opening of image potential state on reconstructed ir(001) surface, Phys. Rev. Res. **7**, 023294 (2025).

[33] H. Ishida, Rashba spin splitting of Shockley surface states on semi-infinite crystals, Physical Review B **90**, 235422 (2014).

[34] H. Ishida, Surface band structure of the reconstructed Ir(001)-(5×1) surface, Surface Science **744**, 122472 (2024).

[35] H. Ishida, Electronic origin of the strongly anisotropic energy dispersion of image potential states at W(110) and Ta(110), Phys. Rev. B **111**, 125408 (2025).

[36] M. Scardamaglia, S. Lisi, S. Lizzit, A. Baraldi, R. Larciprete, C. Mariani, and M. G. Betti, Graphene-induced substrate decoupling and ideal doping of a self-assembled iron-phthalocyanine single layer, The Journal of Physical Chemistry C **117**, 3019 (2013).

[37] A. Varykhalov, D. Marchenko, M. R. Scholz, E. D. L. Rienks, T. K. Kim, G. Bihlmayer, J. Sánchez-Barriga, and O. Rader, Ir(111) Surface State with Giant Rashba Splitting Persists under Graphene in Air, Physical Review Letters **108**, 066804 (2012).

[38] I. Pletikosic, M. Kralj, P. Pervan, R. Brako, J. Coraux, T. N'Diaye A, C. Busse, and T. Michely, Dirac cones and minigaps for graphene on ir(111), Physical Review Letters **102**, 056808 (2009).

[39] M. Petrović, J. T. Sadowski, A. Šiber, and M. Kralj, Wrinkles of graphene on Ir(111): Macroscopic network ordering and internal multi-lobed structure, Carbon **94**, 856 (2015).